chemosensors

MDPI

Article

Digital Morphology Meets Chemometrics: Multi-Sensor Combination for Rapid Quality Grading and Geographical Origin Discrimination of *Atractylodes lancea* Rhizome

Lu Chen *, Changyun Dai, Mingjun Wang, Feilong Ren, Zhiming Zeng and Hui Ao

School of Pharmacy, Chengdu University of Traditional Chinese Medicine, Chengdu 611137, China; dcy0109@stu.cdutcm.edu.cn (C.D.); wangmingjun@stu.cdutcm.edu.cn (M.W.); renfeilong@stu.cdutcm.edu.cn (F.R.); zengzhiming1216@stu.cdutcm.edu.cn (Z.Z.); aohui@cdutcm.edu.cn (H.A.)
* Correspondence: chenlu@cdutcm.edu.cn

Abstract

The dried rhizome of *Atractylodes lancea* (RAL) is a widely used traditional Chinese medicine (TCM). Its quality evaluation and origin authentication have long relied on time-consuming chromatographic methods, which are poorly suited for rapid, on-site decisions in commercial supply chains, and existing studies generally focus on isolated morphological indicators without systematic digital characterization and practical on-site grading tools. Guided by the traditional empirical knowledge of "Bianzhuang Lunzhi", which holds that external morphological traits can reflect the internal quality of TCM, this study presents the first systematic multi-dimensional digital characterization of RAL morphological traits using an integrated multi-sensor approach and quantitatively explores the underlying correlations between digital traits and key bioactive constituent contents. Nighty samples from three major producing regions were analyzed. Significant correlations were observed between odor indices, color parameters, density, oil cavity area ratio and bioactive component contents in the authentic Maoshan-sourced RAL ($p < 0.01$ or $p < 0.05$). Such associations were absent in the emerging regions (Dabie and Qin−Ba Mountains). A three-grade quality classification system based on density thresholds (Grade A: $\geq$0.73 g/cm^3; B: 0.58–0.73 g/cm^3; C: <0.58 g/cm^3) was established specifically for Maoshan RAL. Additionally, an electronic nose-based classification model was constructed for geographical origin discrimination, which delivered reliable and robust classification performance in external validation with independent blind test samples. This work provides practical, low-cost tools for rapid quality grading and origin identification of RAL. The proposed trait-driven analytical strategy offers a generalizable framework for the quality control of other complex herbal medicines.

Keywords: *Atractylodes lancea*; multi-sensor combination; rapid quality grading; geographical origin discrimination

Received: 2 June 2026
Revised: 6 July 2026
Accepted: 10 July 2026
Published: 12 July 2026

1. Introduction

The dried rhizome of *Atractylodes lancea* (Thunb.) DC. (RAL, commonly known as *Maocangzhu*) is a cornerstone medicinal material in traditional Chinese medicine (TCM), widely recognized as the principal remedy for dampness syndromes. Modern phytochemical and pharmacological studies have demonstrated that its principal bioactive components are essential oils, primarily comprising sesquiterpenoids (e.g., atractylone, hinesol, β-eudesmol) and polyacetylenes (e.g., atractylodin) [1], which exhibit prominent anti-inflammatory, antibacterial, antioxidant, and immunomodulatory activities [2–5]. As

a widely used medicinal material, reliable quality evaluation and geographical origin authentication are critical for ensuring its clinical therapeutic efficacy and standardized industrial application [6].

Currently, the quality control and origin tracing of RAL predominantly rely on chromatographic techniques, including gas chromatography–mass spectrometry (GC-MS) and high-performance liquid chromatography (HPLC) [7,8]. Although these methods provide high analytical accuracy, they require complex sample preparation, are time-consuming, costly, and lack portability, which severely limits their application for rapid on-site analysis [8]. In addition, with the continuous expansion of RAL cultivation areas, geographical variations in the chemical profiles of RAL have become increasingly evident, while practical and rapid approaches for origin discrimination remain scarce.

In this context, the traditional empirical knowledge of "Bianzhuang Lunzhi" offers a promising conceptual framework for addressing these challenges. At its core, this empirical principle holds that macroscopic morphological traits, such as shape, color, density, texture and aroma, closely correlate with the internal quality of medicinal materials, thereby enabling rapid quality assessment based on these readily observable sensory characteristics [9]. In the case of RAL, traditional empirical knowledge holds that superior quality is characterized by a firmer texture, a denser distribution of oil cavities (cinnabar-like dots), and a more intense aroma. However, such qualitative evaluations have long relied on subjective sensory assessments and the experience of TCM practitioners, lacking systematic validation using modern analytical techniques, and consequently have not developed into objective, quantifiable, and standardized criteria. In recent years, the rapid development of bionic sensors—including colorimeters, image analysis systems, and electronic noses—has made it possible to simulate human visual and olfactory perception, transforming subjective sensory attributes into precise, digitized parameters [10–12]. Integrating these multi-dimensional characterization techniques with chemometric approaches not only offers a reliable way to scientifically validate the "Bianzhuang Lunzhi" empirical principle but also shows great potential for developing rapid, practical methods for quality evaluation and origin authentication of RAL.

In this study, the relationship between morphological traits and the contents of major active essential oil constituents in RAL was systematically investigated by combining multi-sensor technologies and chemometric methods (Figure 1). A total of 90 RAL samples from three major producing regions were included, among which 80 were used for core analysis and 10 served as independent blind validation samples. The primary objectives of this study were twofold: (i) to quantitatively evaluate the correlation between key morphological indicators (including density, oil chamber characteristics, color, and odor) and the contents of active components, thereby providing empirical support for the "Bianzhuang Lunzhi" principle; and (ii) to explore the potential of these measurable traits for developing rapid and practical approaches to quality grading and geographical origin authentication of RAL. This work establishes a data-driven framework to advance the standardization and on-site application of quality assessment for this clinically important medicinal herb.

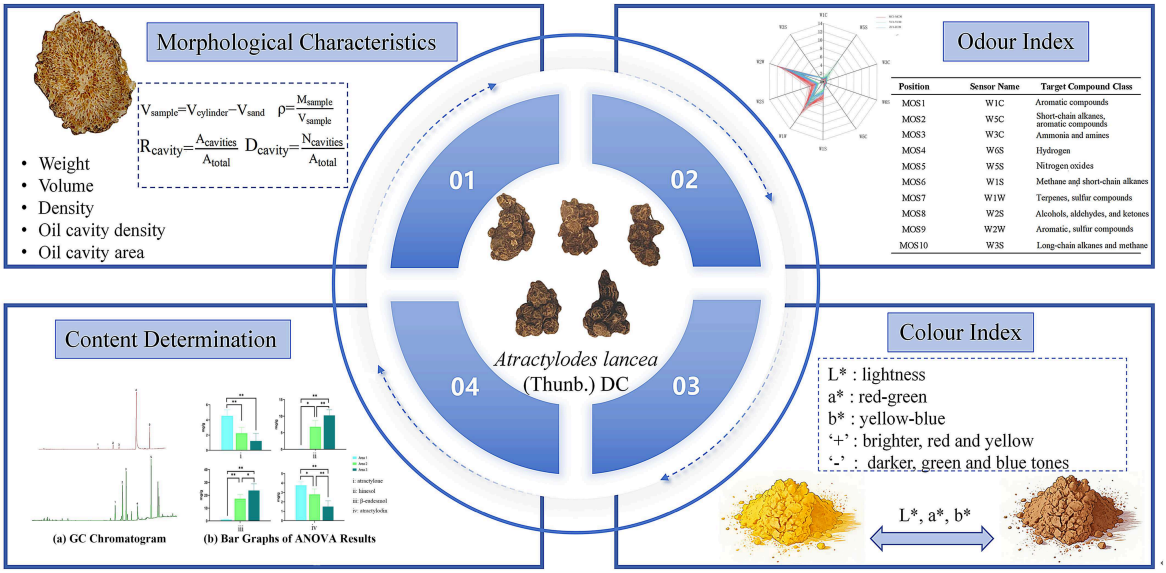

Figure 1. Schematic diagram of the multi-dimensional characterization system for RAL. * $p < 0.05$, ** $p < 0.01$.

2. Materials and Methods

2.1. Materials and Reagents

Chemicals: atractylone (purity ≥ 98%, Batch No. MUST-24042301), atractylodin (purity ≥ 98%, Batch No. MUST-24041804), and β-eudesmol (purity ≥ 98%, Batch No. MUST-24011607) were supplied by Chengdu Manst Biotechnology Co., Ltd. (Chengdu, China). Hinesol (purity ≥ 97%, Batch No. AFBF3002) was provided by Chengdu Alfalfa Biotechnology Co., Ltd. (Chengdu, China). n-Hexane (HPLC grade) was obtained from Thermo Fisher Scientific Inc. (Shanghai, China). Ultrapure water was prepared using a Milli-Q water purification system (Millipore, Burlington, MA, USA).

Plant Materials: A total of 90 samples of RAL were collected for this experiment, all cultivated samples aged three years old. These comprised 34 samples from the Maoshan region in Jiangsu Province (MC01–MC34), 34 samples from the Dabie Mountains (YC01–YC34), and 22 samples from the Qin−Ba Mountains (ZC01–ZC22), as detailed in Table S1. All samples, upon collection from their producing areas, were immediately placed in a constant-temperature oven at 45 °C for drying until constant weight, then transferred to a desiccator containing indicating silica gel for hermetic storage until use. All 90 samples were randomly divided into two subsets prior to formal analysis: a core analysis set (80 samples) and an independent external blind validation set (10 samples). The core analysis set consisted of 30 samples from Maoshan, 30 from the Dabie Mountains, and 20 from the Qin−Ba Mountains, which were used for morphological trait determination, volatile component quantification, trait–component correlation analysis, and discriminant model training. The remaining 10 samples (4 from Maoshan, 4 from the Dabie Mountains, 2 from the Qin−Ba Mountains) served as the blind validation set. This subset was completely isolated from all feature extraction, correlation analysis, and model training procedures and was only used for the final external validation to ensure an unbiased evaluation of model generalization performance.

2.2. Weight Determination

The weight of samples was measured using an analytical balance with a precision of 0.001 g. Three representative samples were randomly selected from each producing area, and the moisture content was determined by the toluene method in accordance

with General Rule 0832 of the Chinese Pharmacopoeia (2025 Edition), with three parallel determinations performed for each sample. The sample weight (M_{sample}) was calculated on a dry weight basis, i.e., the measured values were corrected by subtracting the moisture content of the samples.

2.3. Density Measurement

After recording the sample mass (M_{sample}), the sample was transferred into a calibrated graduated cylinder, and pretreated fine sand was added to fill the voids and ensure complete submersion of the sample. The fine sand used in the experiment was commercial analytical-grade quartz sand with a particle size of 0.25~0.50 mm (passed through a 40~60 mesh sieve). Prior to use, the fine sand was washed with deionized water, dried in a forced-air oven at 105 °C for 4 h, and sieved again to ensure uniform particle size, as well as to remove residual moisture and impurities that might impair the accuracy of volume measurement. The pretreated fine sand was added to the graduated cylinder containing the sample in increments; after each addition, the cylinder was gently tapped and manually swirled for 2~3 min. This operation was repeated until the sand surface stabilized and the total volume no longer decreased, with confirmation that all voids were fully filled, no exposed parts of the sample existed, and no air bubbles were present in the system. The scale reading of the cylinder at this point was recorded as the total volume (V_{total}). The sample and fine sand were poured out of the cylinder, the sample was separated, and the fine sand adhering to its surface was removed. The recovered fine sand was then poured back into the original calibrated graduated cylinder, gently tapped and manually swirled for 2~3 min using the same procedure until the volume stabilized, and the stable volume at this point was recorded as the volume of fine sand alone (V_{sand}). The sample volume (V_{sample}) was calculated as

$$V_{sample} = V_{total} - V_{sand}$$

where V_{total} denotes the total volume of fine sand and RAL in the graduated cylinder, and V_{sand} denotes the volume of fine sand alone under the same experimental conditions.

Density (ρ) was then determined by

$$\rho = \frac{M_{sample}}{V_{sample}}$$

Three independent replicate measurements were performed for each sample, and the mean value was reported as the final density [13].

2.4. Determination of Oil Cavity Area Ratio and Density in Cross-Section

Transverse sections were obtained from the region of maximum diameter of RAL according to a previously reported method [14]. The sections were placed on a neutral white background and photographed under uniform diffuse illumination using a high-resolution digital camera positioned orthogonally to the sample plane. Based on the core principle that oil cavity structures can be accurately identified via binary image conversion through threshold segmentation, the total cross-sectional area (A_{total}) and total area of oil cavities (A_{cavity}) were quantified using ImageJ software (version 1.53, National Institutes of Health, Bethesda, MD, USA). Briefly, the original microscopic images were uniformly converted into 8-bit grayscale images, followed by global spatial scale calibration based on the standard scale bar. Unbiased segmentation between oil cavities and background tissue was completed using Otsu's automatic thresholding method. Automated counting and area measurement of oil cavities with an area greater than 50 μm^2 were performed via the built-in "Analyze Particles" module of the software. Meanwhile, the total cross-sectional area of the tissue field of view (A_{total}) and the total area of all quantified oil cavities (A_{cavity})

were acquired (Figure 2). Finally, the oil cavity area ratio and cross-sectional oil cavity density were calculated accordingly. All samples were analyzed using identical procedures and parameters to ensure the reproducibility of the results. The oil cavity area ratio (R_{cavity}) was calculated as

$$R_{cavity} = \frac{A_{cavity}}{A_{total}}$$

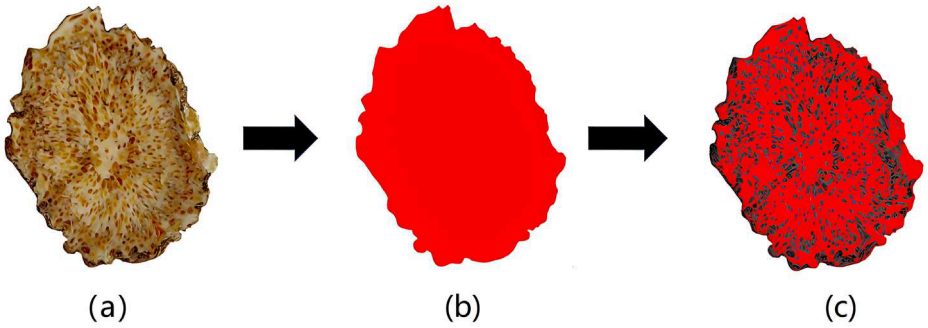

Figure 2. Schematic diagram of oil cavity area and density measurement in RAL cross-sections using ImageJ software. (**a**) Original microscopic image of a RAL transverse section. (**b**) Segmentation of the total tissue area (red region). (**c**) Segmentation of oil cavity structures (dark blue regions within the red tissue area).

Concurrently, the number of oil cavities in each cross-section was counted using the same particle analysis module. The cross-section oil cavity density (D_{cavity}) was determined by

$$D_{cavity} = \frac{N_{cavity}}{A_{total}}$$

2.5. Color Difference Measurement

The RAL samples were dried to constant weight at 45 °C, then pulverized and passed through an 80-mesh sieve to yield a homogeneous powder. The color parameters of RAL powder were measured using a CM-5 benchtop spectrophotometer (Konica Minolta, Tokyo, Japan) according to a previously reported method [15], with the following settings: D65 standard illuminant, 10° observer angle, and 30 mm measurement aperture. The instrument employed LED-based illumination. Color values were quantified in the CIELAB color space (L*, a*, b*), where L* represented lightness, a* indicated the red-green coordinate (positive values toward red, negative toward green), and b* denoted the yellow-blue coordinate (positive values toward yellow, negative toward blue). Prior to measurement, the instrument was calibrated using standard white and black reference tiles. Three replicate measurements were performed for each sample, and the mean L*, a*, and b* values were recorded.

2.6. Electronic Nose Measurement

Volatile compound profiles of RAL were characterized using a PEN3 electronic nose system (Airsense GmbH, Schwerin, Germany). Powdered samples (1.0 g) were precisely weighed into 15.0 mL headspace vials and immediately sealed with PTFE/silicone septum caps. Dynamic headspace sampling was performed at ambient temperature (25 ± 1 °C), where headspace volatiles were carried to the sensor array by high-purity air at a flow rate of 600.0 mL·min^{-1}. The measurement protocol consisted of 5.0 s sensor stabilization, 120.0 s data acquisition (with 1.0 s sampling intervals), and 100.0 s automated purge between measurements. The characteristics of the 10-metal oxide semiconductor sensor array are presented in Table 1. Each sample was analysed in triplicate, with the mean value recorded.

The "odor index" was calculated as the sum of response values from all 10 sensors and was used to quantitatively represent the overall volatile intensity of each sample.

Table 1. PEN3 Electronic Nose Sensor Array Characteristics and Detection Ranges.

Position	Sensor Name	Target Compound Class
MOS1	W1C	Aromatic compounds
MOS2	W5C	Short-chain alkanes, aromatic compounds
MOS3	W3C	Ammonia and amines
MOS4	W6S	Hydrogen
MOS5	W5S	Nitrogen oxides
MOS6	W1S	Methane and short-chain alkanes
MOS7	W1W	Terpenes, sulfur compounds
MOS8	W2S	Alcohols, aldehydes, and ketones
MOS9	W2W	Aromatic and sulfur compounds
MOS10	W3S	Long-chain alkanes and methane

2.7. GC-MS Analysis

Sample Preparation: Accurately weighed 1.000 g of RAL powder was placed in a stoppered Erlenmeyer flask, and 10 mL of n-hexane was accurately added. The total mass of the mixture was precisely weighed and recorded. The mixture was sonicated for 30 min at a power of 250 W and a frequency of 40 kHz. After cooling to room temperature, n-hexane was added to compensate for the mass loss incurred during sonication, bringing the total mass of the mixture back to the initial value recorded prior to sonication. The mixture was filtered through a 0.22 μm organic phase microporous membrane, and the subsequent filtrate was collected as the test solution, which was stored in a refrigerator at 4 °C. Prior to use, the test solution was appropriately diluted according to its actual concentration to ensure that the analyte concentration fell within the linear range of the standard curve before instrumental detection.

Chromatographic Conditions: Adapted from the method reported by Zhang et al. [16]. Analyses were performed on an Agilent 7890A-5975C GC-MS system (Agilent Technologies, Santa Clara, CA, USA) fitted with an HP-5 MS capillary column (30 m × 0.25 mm × 0.25 μm). The injector temperature was set at 250 °C. The oven temperature program was programmed as follows: an initial temperature of 100 °C, increased to 135 °C at 10 °C·min^{-1}, then to 145 °C at 0.5 °C·min^{-1} (held for 6 min), and finally to 250 °C (held for 8 min). High-purity helium (purity ≥ 99.999%) was used as the carrier gas at a constant flow rate of 1.0 mL·min^{-1}. Samples were injected in split mode with a split ratio of 50:1 and an injection volume of 1 μL. Mass spectrometry conditions included electron ionization mode at 70 eV, with both ion source and transfer line temperatures maintained at 250 °C.

Method validation was carried out in full compliance with ICH Q2(R1) guidelines for the four target analytes (atractylone, hinesol, β-eudesmol, and atractylodin), which were quantified via the external standard method with GC-MS operated in full scan (SCAN) mode. All analytes exhibited excellent linearity between injection concentration and corresponding peak area within their respective ranges (atractylone 0.00502–0.502 mg/mL, hinesol 0.00300–0.300 mg/mL, β-eudesmol 0.00498–0.498 mg/mL, atractylodin 0.00504–0.504 mg/mL), with correlation coefficients (R^2) ranging from 0.9980 to 0.9988. For all target compounds, the relative standard deviation (RSD) values of instrument precision (6 consecutive injections, n = 6), method repeatability (6 parallel preparations, n = 6), and 24 h room-temperature stability of test solution (n = 6) were all below 5.0%. The spiked recovery test was performed at low, medium and high concentration levels for each analyte, with 3 parallel samples prepared for each level. The spiked recoveries of all four target analytes were within the range from 92.84% to 105.67%, with

the relative standard deviation (RSD) of recovery at each level below 5.0%. The method showed good specificity, with no interfering chromatographic peaks at the retention times of the four target analytes in blank solvent and sample matrix. Detailed calibration curve parameters and complete validation datasets are provided in Table S1.

2.8. Data Analysis

To eliminate dimensional and magnitude-based discrepancies among different indicators for multivariate statistical analysis, all data were standardized via z-score transformation, with the formula: z-score = $(x - \mu)/\sigma$, where x denotes the original value, μ the mean of the dataset, and σ the standard deviation. ANOVA followed by Tukey's post hoc test for multiple comparisons was used to evaluate the differences in bioactive component contents among RAL samples from different producing regions. Spearman rank correlation analysis was performed to assess the correlation between morphological traits and bioactive component contents, with all analyses conducted independently for samples from each producing region. A two-tailed test was used for all correlation analyses, with a p-value < 0.05 defined as statistically significant, and a p-value < 0.01 was defined as highly statistically significant. To control the Type I error rate induced by multiple correlation tests, the Benjamini–Hochberg false discovery rate (FDR) adjustment was applied to all p-values generated from the correlation analyses. Statistical significance was determined based on the FDR-adjusted p-values, with an adjusted p-value < 0.05 set as the threshold for significance. The strength of the Spearman rank correlation coefficient (r_s) was classified according to the internationally recognized Cohen's standard: $|r_s| \geq 0.7$ was defined as a strong correlation, $0.5 \leq |r_s| < 0.7$ as a moderate correlation, and $0.3 \leq |r_s| < 0.5$ as a weak correlation. Correlations with $|r_s| < 0.3$ were considered to have no practical application value, even if statistically significant. Statistical analyses, including HCA and K-means clustering analysis (K = 3), were performed using SPSS 23.0 (IBM, Armonk, NY, USA). For the verification of the density-based quality grading system, both external validation with independent test samples and leave-one-out cross-validation (LOOCV) were adopted. For external validation, samples not involved in the establishment of the grading threshold were used to evaluate the practical discriminative performance of the criteria. For LOOCV, one sample was excluded from the modeling set in each iteration, the grading threshold was re-established based on the remaining samples, and the grade of the excluded sample was predicted; the overall grade prediction consistency rate was calculated after all cycles to assess the robustness of the grading standard.

For electronic nose dataset processing, SPSS 23.0 was also adopted to conduct PCA dimensionality reduction and construct the primary DFA geographical origin discrimination model. To further verify the robustness of the discrimination results, a parallel partial least squares discriminant analysis (PLS-DA) model was built, coupled with leave-one-out cross-validation (LOOCV). LOOCV was implemented on the 80 training samples to assess the model's generalization ability and alleviate overfitting risks within a limited sample size. In each iteration, one sample was separated as the validation subset, with the rest used for model training. The iterative process continued until each sample underwent independent validation once. All classification outcomes were compiled to generate a confusion matrix, from which the overall cross-validation accuracy was computed.

3. Results

3.1. Digital Morphological Traits of RAL

Eighty samples of RAL were collected from three major producing areas (MC01–MC30: Maoshan region; YC01–YC30: Dabie Mountains; ZC01–ZC20: Qin−Ba Mountains). Nine morphological parameters, including weight, volume, density, R_{cavity}, D_{cavity}, the CIELAB

color parameters (L*, a*, b*), and the odor index (Figure 3a), were systematically determined. The complete morphological dataset is presented in Table S2.

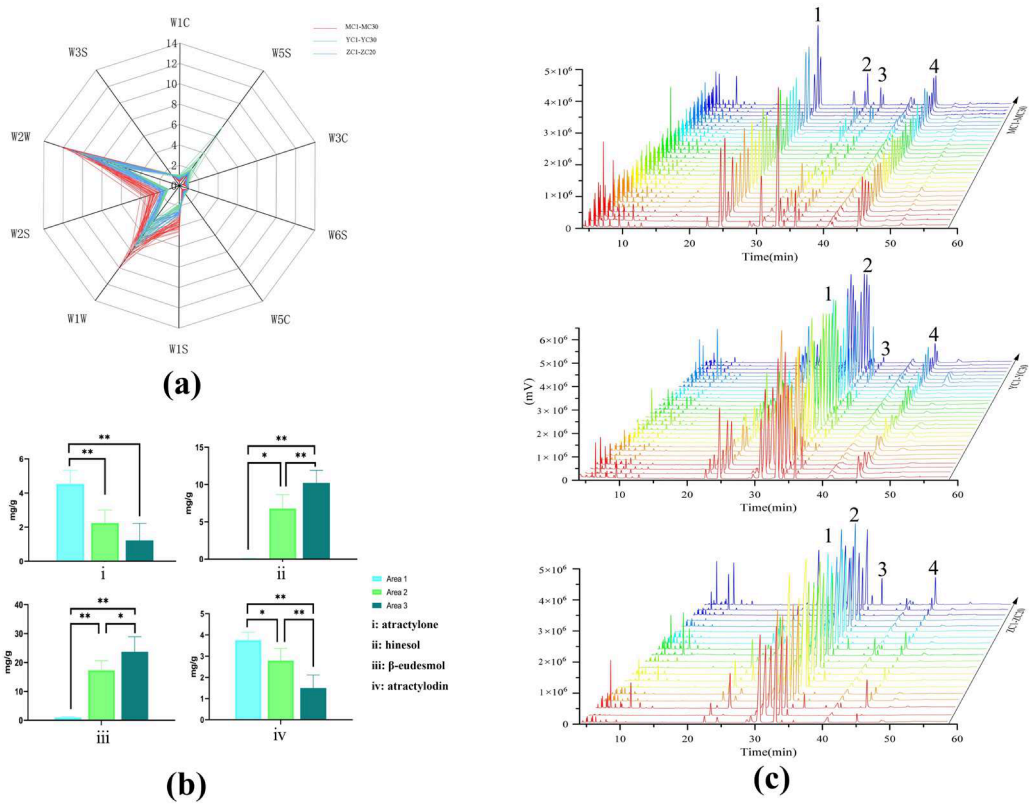

Figure 3. Comprehensive characterization of morphological, odor, and chemical traits of RAL. (**a**) Radar plot of electronic nose sensor responses for RAL from the Maoshan (MC), Dabie Mountains (YC), and Qin−Ba Mountains (ZC). (**b**) GC-MS total ion chromatograms (TICs) of RAL samples, with peaks identified as: i. atractylone, ii. hinesol, iii. β-eudesmol, iv. atractylodin. (**c**) Inter-region comparison of four bioactive component contents via ANOVA (1: atractylone, 2: hinesol, 3: β-eudesmol, 4: atractylodin; y-axis: content in mg/g, dry weight; * $p < 0.05$, ** $p < 0.01$). (Area 1: Maoshan, Area 2: Dabie Mountains, Area 3: Qin−Ba Mountains).

3.2. Analysis of Active Components

Four key bioactive components (atractylone, hinesol, β-eudesmol, atractylodin) were quantified by GC-MS. The total ion chromatograms are shown in Figure 3b, and the content data of each sample are summarized in Table S3.

A one-way analysis of variance (ANOVA) followed by Tukey's post hoc test was performed to compare inter-group differences, which revealed statistically significant ($p < 0.05$) or highly statistically significant ($p < 0.01$) differences in the contents of the four active components among RAL from the three producing areas, indicating distinct chemotypic profiles (Figure 3c), which is consistent with previously reported findings [8]. Specifically, the volatile oil of Maoshan-sourced RAL was dominated by atractylone (4.53 ± 2.14 mg/g) and atractylodin (3.76 ± 1.00 mg/g), with the contents of both components significantly higher than those in samples from the Dabie Mountains and Qin−Ba Mountains ($p < 0.05$). In contrast, the volatile oil of RAL from the Dabie Mountains and Qin-Ba Mountains was characterized by hinesol and β-eudesmol as dominant components. For Qin−Ba Mountains samples, the contents of hinesol (10.21 ± 3.62 mg/g) and β-eudesmol (23.69 ± 11.10 mg/g) were significantly higher than those in Dabie Mountains samples (6.80 ± 4.97 mg/g and 17.34 ± 8.81 mg/g, $p < 0.05$), while the atractylodin content (1.50 ± 1.32 mg/g) was highly significantly lower than that in Dabie Mountains (2.80 ± 1.52 mg/g, $p < 0.01$).

3.3. Correlation Analysis

All Spearman rank correlation analyses were conducted independently for RAL samples from each producing region (30 batches from the Maoshan region, 30 batches from the Dabie Mountains, and 20 batches from the Qin−Ba Mountains). The Benjamini–Hochberg false discovery rate (FDR) adjustment was applied to all correlation *p*-values within each region to control the Type I error rate induced by multiple tests, and statistical significance was uniformly determined based on FDR-adjusted *p*-values.

For RAL from the Maoshan region, significant multi-dimensional correlations were observed between morphological traits and key bioactive components (Figure 4: Area 1). All core correlation findings remained statistically robust after FDR correction. Density exhibited a strong, highly statistically significant positive correlation with the total content of the four bioactive components (r_s = 0.877, $p < 0.01$). Specifically, density showed strong positive correlations with atractylone (r_s = 0.836, $p < 0.01$) and atractylodin (r_s = 0.733, $p < 0.01$), a moderate positive correlation with hinesol (r_s = 0.653, $p < 0.01$), and a weak positive correlation with β-eudesmol (r_s = 0.367, $p < 0.05$). R_{cavity} also showed highly statistically significant moderate-to-strong positive correlations with the contents of atractylone, β-eudesmol, hinesol, atractylodin, and their total content (r_s = 0.54–0.84, $p < 0.01$). In addition, the electronic nose odor index showed statistically significant moderate positive correlations with the contents of atractylone and atractylodin (r_s = 0.42–0.49, $p < 0.05$). The color parameter L* (lightness) showed statistically significant to highly statistically significant moderate-to-strong negative correlations with atractylone, hinesol, β-eudesmol, atractylodin, and the total content of the four components (r_s = −0.44~−0.84, $p < 0.05$ or $p < 0.01$).

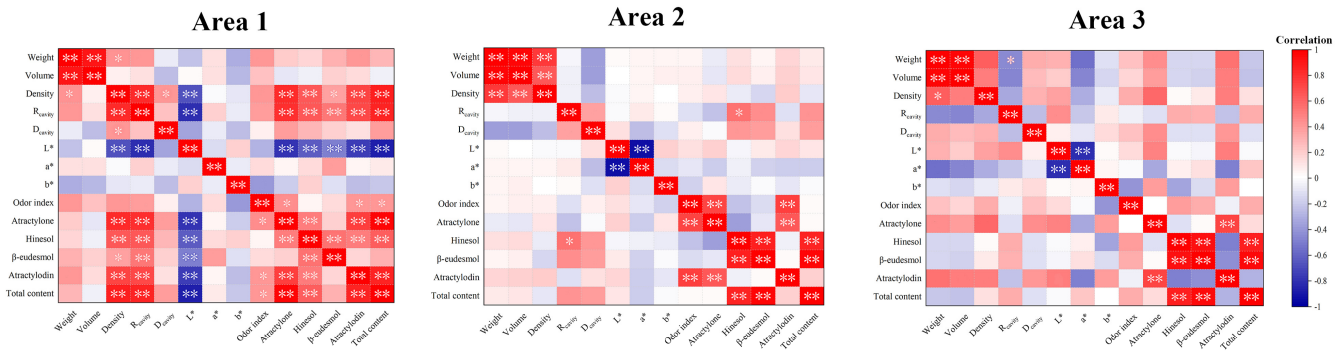

Figure 4. Spearman rank correlation heatmaps of morphological traits vs. bioactive component contents for each producing region. (Area 1: Maoshan, Area 2: Dabie Mountains, Area 3: Qin−Ba Mountains. Color scale indicates Spearman correlation coefficient (r_s): red = positive correlation, blue = negative correlation. * $p < 0.05$, ** $p < 0.01$).

In samples from the Dabie Mountains, raw correlation analysis showed that R_{cavity} and D_{cavity} exhibited weak-to-moderate positive correlations with hinesol, β-eudesmol, and the total content of the four bioactive constituents (r_s = 0.39–0.55, $p < 0.01$ or $p < 0.05$). However, after the Benjamini–Hochberg FDR adjustment, most of these scattered weak associations no longer reached the statistical significance threshold. No statistically significant associations (adjusted $p > 0.05$) were detected between the other morphological traits—including weight, volume, density, color parameters (L, a, b*), and electronic nose odor index—and any individual or total bioactive constituents (Figure 4: Area 2).

In Qin−Ba Mountain samples, raw correlation results indicated that atractylone content showed moderate positive correlations with sample weight, density, oil cavity density, and L value (r_s = 0.45–0.60, $p < 0.05$ or $p < 0.01$). Atractylodin content was moderately positively associated with weight, volume, density, and L (r_s = 0.51–0.56, $p < 0.05$) and

moderately negatively correlated with a* ($r_s = -0.49$, $p < 0.05$). After FDR adjustment, the majority of these isolated correlations failed to meet the significance criterion. No significant relationships ($p > 0.05$) were found between the total content of the four constituents and any morphological traits (Figure 4: Area 3).

3.4. Density-Based Classification of Maoshan-Sourced RAL

3.4.1. Screening of Grading Index

Based on the correlation analysis results in Section 3.3, density was selected as the core index for quality grading of Maoshan-sourced RAL, with the following screening criteria: (1) Strongest correlation: density showed highly significant positive correlations with atractylone, hinesol, atractylodin, and total content ($p < 0.01$), with correlation coefficients (r_s) of 0.836, 0.653, 0.733, and 0.877, respectively; (2) Convenient operation: the detection time for a single sample was <3 min, much shorter than that of conventional HPLC/GC-MS detection (>2 h per sample); (3) Good repeatability: the relative standard deviation (RSD) of parallel measurements was <3% ($n = 3$), with low requirements for the professional skills of operators.

3.4.2. K-Means Cluster Analysis and Establishment of Grading Standard

K-means cluster analysis was performed on 30 batches of Maoshan-sourced RAL samples, with density as the sole clustering variable. Prior to clustering, Z-score standardization was performed on the density dataset, with a mean density of 0.689 g·cm^{-3} and a standard deviation of 0.101 g·cm^{-3}. The random seed was fixed during the whole analysis process to ensure the repeatability of clustering results. The optimal cluster number $K = 3$ was determined by the Elbow Method and Silhouette Coefficient Method. The Elbow Method showed a clear inflection point at $K = 3$, where the decline rate of within-cluster sum of squares (inertia) slowed down significantly. The average Silhouette Coefficient for K values ranging from 2 to 6 was calculated, and the highest coefficient was obtained at $K = 3$ (silhouette coefficient = 0.621, indicating good clustering stability), indicating a well-defined clustering structure with tight intra-cluster cohesion and clear inter-cluster separation. The optimal cluster number $K = 3$ was finally determined, which was also consistent with the conventional three-grade classification system for commercial Chinese medicinal materials.

The clustering results showed that the density cluster centers of the three clusters were 0.7838, 0.6540, and 0.5247 g/cm^3, respectively. Combined with the natural breakpoints of the actual density dataset, the final cut-off thresholds between adjacent grades were set as 0.73 g/cm^3 and 0.58 g/cm^3 (Table 2).

Table 2. Density clustering results of Maoshan-sourced RAL (g/cm^3).

Cluster Group	Number of Samples	Density Range [1]	Cluster Center [1]	Cut-Off Threshold Between Adjacent Clusters [1]
Cluster 1	13	0.7397–0.8761	0.7838	0.73
Cluster 2	12	0.5985–0.7183	0.6540	0.58
Cluster 3	5	0.5052–0.5617	0.5247	

[1] Unit: g/cm^3.

In accordance with the conventional three-grade classification standard for Chinese medicinal materials and verified by the significant gradient differences in the contents of key active components among the three grades, a three-grade quality grading system for Maoshan-sourced RAL based on density was established: Grade A (density $\geq$ 0.73 g/cm^3),

Grade B (0.58 ≤ density < 0.73 g/cm^3), and Grade C (density < 0.58 g/cm^3). The corresponding bioactive component contents of each grade are shown in Table 3.

Table 3. Density-based quality grade standard of Maoshan-sourced RAL.

Quality Grade	Density [1]	Atractylone [2]	Hinesol [2]	β-Eudesmol [2]	Atractylodin [2]
Grade A	≥0.73	6.27 ± 1.56	0.13 ± 0.03	1.21 ± 0.92	4.43 ± 0.84
Grade B	0.58~0.73	3.66 ± 1.26	0.07 ± 0.04	0.97 ± 0.53	3.65 ± 0.71
Grade C	<0.58	1.93 ± 0.97	0.04 ± 0.02	0.53 ± 0.18	2.26 ± 0.46

[1] Unit: g/cm^3. [2] Contents for atractylone, hinesol, β-eudesmol, and atractylodin are expressed in mg/g.

3.4.3. Verification of the Density-Based Quality Grading System

ANOVA results showed that there were extremely statistically significant differences in the contents of atractylone, hinesol, β-eudesmol, atractylodin, and their total content among the three quality grades of RAL ($p < 0.001$, Table 4). Tukey's post hoc multiple comparisons further confirmed that the pairwise comparisons of the total content of the four bioactive components among Grade A, Grade B and Grade C all reached a statistically significant level ($p < 0.05$, Table 4). Meanwhile, the contents of the four individual bioactive components also showed a consistent downward gradient trend from Grade A to Grade C, which fully verified the rationality of the grading standard. The above results indicated that the established density-based three-grade grading system can effectively distinguish Maoshan-sourced RAL with different intrinsic quality levels.

Table 4. ANOVA and Tukey's results for Maoshan-sourced RAL quality grades.

Index	Grade A [1]	Grade B [1]	Grade C [1]	ANOVA (*F*-Value/*p*-Value)	Tukey's Post Hoc (*p*-Value) [2]
Total content	12.04 ± 2.30	8.34 ± 1.97	4.96 ± 0.71	25.242/<0.001	A > B ($p < 0.001$) B > C ($p = 0.01$) A > C ($p < 0.001$)

[1] Contents are expressed in mg/g as mean ± standard deviation (SD). [2] $p < 0.05$ was considered statistically significant.

To further evaluate the generalization ability and robustness of the established grading system, external validation with independent samples and leave-one-out cross-validation (LOOCV) were additionally performed. For external validation, 4 independent Maoshan RAL samples that did not participate in K-means clustering and threshold construction were used as the test set. The grading results determined by the pre-established density thresholds were fully consistent with the actual quality levels reflected by the total bioactive component content, directly confirming the practical discriminative performance of the grading standard on independent samples (detailed data are provided in Table S6). Meanwhile, LOOCV was conducted on the 30 modeling samples to verify the stability of the grading threshold. After 30 cycles of iterative verification, the overall consistency rate of grade prediction reached 93.3% (Figure S1), indicating that the density-based three-grade grading system has satisfactory robustness and is not susceptible to bias caused by individual sample fluctuations.

3.5. Construction and Validation of Geographical Origin Authentication Model for RAL Based on Electronic Nose

3.5.1. Differences in Electronic Nose Odor Characteristics of RAL from Different Geographical Origins

Significant differences in the electronic nose odor fingerprints of RAL from three geographical origins were observed (Figure 3a). One-way ANOVA followed by Tukey's

post hoc test showed that the signal intensities of the W1W, W2W, and W2S sensors for Maoshan-sourced samples were significantly higher than those from the Dabie Mountains and the Qin−Ba Mountains ($p < 0.05$). Meanwhile, the signal intensities of the W5C and W1C sensors for Dabie Mountains-sourced samples were significantly higher than those for samples from the other two origins ($p < 0.05$).

3.5.2. Construction of Geographical Origin Discrimination Model Based on PCA-DFA

PCA was performed on the 10 odor characteristic signals from the electronic nose, and the results showed that the first two principal components (PC1 and PC2) explained 66.86% and 14.73% of the total variance, respectively, with a cumulative explained variance of 81.59%, which could effectively represent the core odor information of RAL samples.

A discriminant function analysis (DFA) model was established based on the first two principal components extracted by principal component analysis (PCA). The first two discriminant functions (DF1 and DF2) explained 82.38% and 17.62% of the total between-group variance, respectively, with a cumulative explanation rate of 100%. The DFA score plot showed that Maoshan-sourced samples were completely separated from samples from the other two origins, while a small overlap was observed between samples from the Dabie Mountains and the Qin−Ba Mountains (Figure 5a).

3.5.3. Blind Test Validation of the Origin Discrimination Model

A total of 90 RAL samples were divided into two subsets: 80 samples for model training and the remaining 10 samples for blind external validation. Ten independent blind test samples (4 batches from the Maoshan region, 4 batches from the Dabie Mountains, 2 batches from the Qin−Ba Mountains) were adopted for external validation. These samples were excluded from the dataset for model training, PCA feature extraction and DFA modeling. The results demonstrated that all 10 blind samples were correctly classified to their actual geographical origins with no misclassification, yielding an overall prediction accuracy of 100% (Figure 5b). The average confidence value calculated based on Mahalanobis distance was 0.9989, and the confidence score of each sample exceeded 0.9.

3.5.4. PLS-DA Model Construction and LOOCV

To further verify the robustness of geographical origin discrimination and evaluate the potential overfitting risk, a PLS-DA model was constructed as a parallel comparison based on electronic nose odor fingerprints.

As shown in the PLS-DA score plot (Figure 5), samples from the three producing regions presented clear clustering patterns with favorable intra-group aggregation. The 95% confidence ellipse of Maoshan samples was completely separated from those of the other two regions, while a slight overlap was observed between the confidence ellipses of Dabie Mountains and Qin−Ba Mountains samples, which was highly consistent with the separation trend observed in the DFA model. After projecting the 10 independent blind test samples into the established PLS-DA model, all samples were correctly assigned to their actual geographical origins, achieving an external validation accuracy of 100%, which was fully consistent with the DFA results.

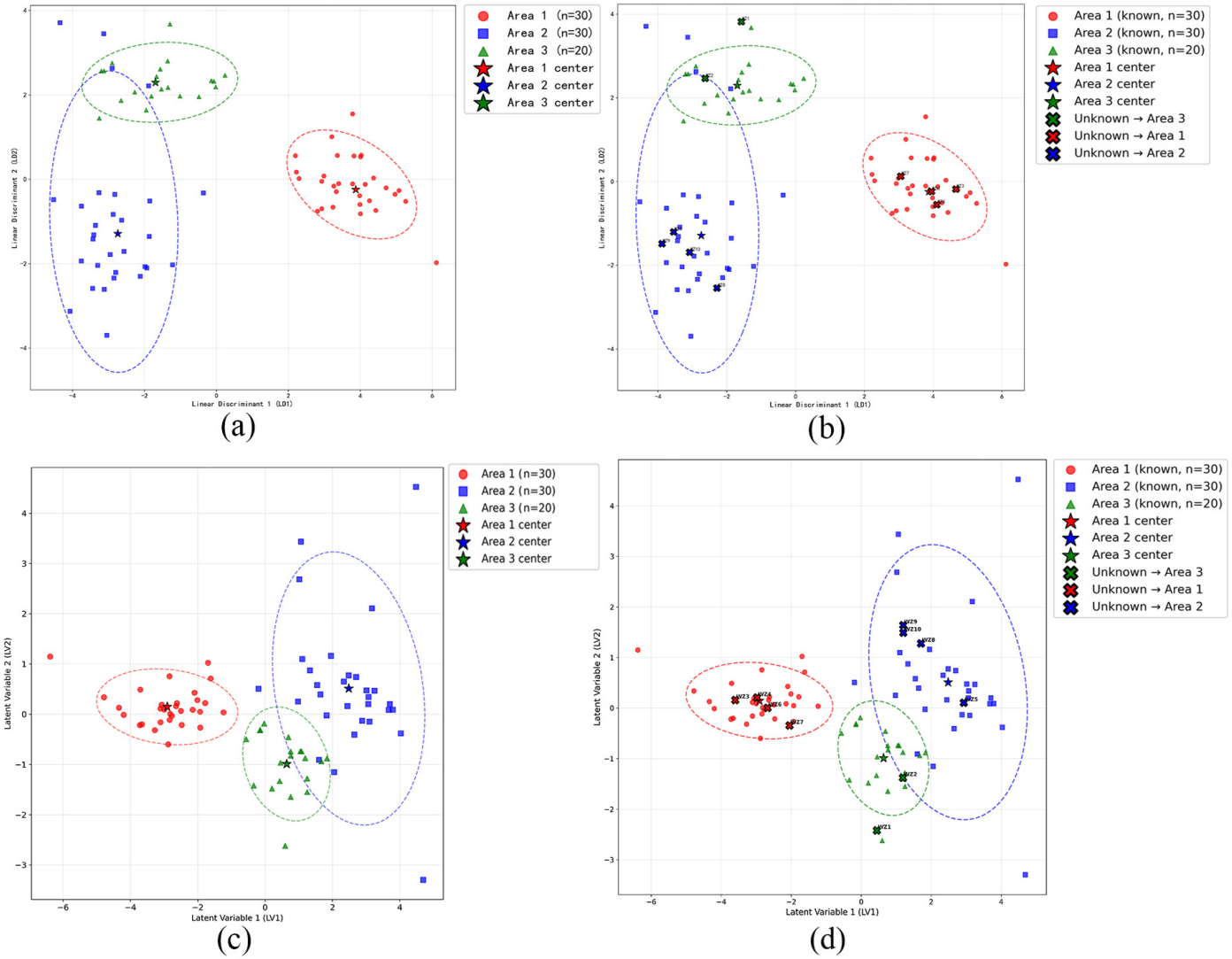

Figure 5. Construction and external validation of the DFA and PLS-DA geographical origin discrimination model for RAL. (**a**) DFA score plot for geographical origin discrimination based on 80 known-origin samples. (**b**) External validation of the DFA model with 10 independent blind test samples. (**c**) PLS-DA score plot for geographical origin discrimination. (**d**) External validation of the PLS-DA model with 10 independent blind test samples.

Furthermore, LOOCV was performed on the 80-sample training set to assess the internal generalization performance of the model. The corresponding confusion matrix (Figure 6) showed that all 30 samples from the Maoshan region were correctly classified with a class-specific accuracy of 100%. For Dabie Mountains samples, 25 out of 30 were correctly discriminated; for Qin−Ba Mountains samples, 19 out of 20 were correctly discriminated. The overall LOOCV accuracy reached 92.5%. Misclassifications only occurred between Dabie Mountains and Qin−Ba Mountains samples, which corresponded to the partial overlap of their volatile component profiles. As the most stringent cross-validation strategy for small-sample scenarios, this high LOOCV accuracy confirmed that the model had favorable generalization ability with no significant overfitting risk.

The highly consistent discrimination performance of the PLS-DA and DFA models mutually corroborated the reliability of the geographical origin authentication results, effectively improving the robustness of the conclusion.

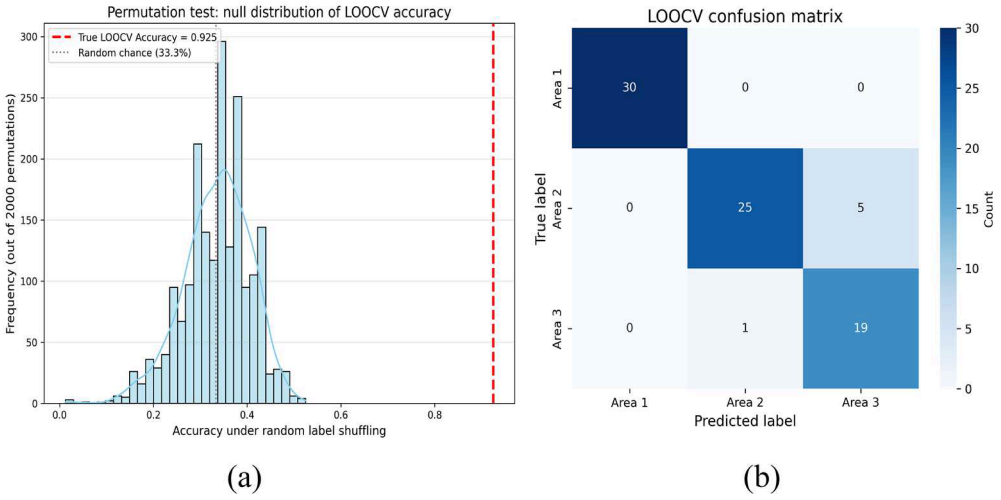

Figure 6. Robustness validation of the PLS-DA geographical origin discrimination model for RAL. (**a**) Null distribution of LOOCV accuracy from 2000 random label permutation tests. (**b**) Confusion matrix of the classification results derived from LOOCV.

4. Discussion

4.1. Trait-Component Correlations

As shown in Figure 4 (Area 1), strong multi-dimensional correlations existed between the morphological traits and key bioactive components of RAL from the Maoshan region. Density and R_{cavity} exhibited significant moderate-to-strong positive correlations with atractylone, β-eudesmol, hinesol, and atractylodin (r_s = 0.54–0.83, $p < 0.01$ or $p < 0.05$). The electronic nose odor index similarly showed significant moderate positive correlations with atractylone, atractylodin, and the total content of these four constituents (r_s = 0.42–0.49, $p < 0.05$). These findings corroborated the traditional empirical principle that compact texture, abundant red oil cavities, and intense aroma signify superior quality. In contrast, the L* value (lightness) displayed highly significant negative correlations with multiple constituents ($p < 0.01$), indicating that darker powder color is associated with higher bioactive content—as a tentative hypothesis, this pattern may be related to the strong light-absorbing properties of concentrated terpenoids, which remain to be further verified.

In contrast, analyses of samples from emerging production areas such as the Dabie Mountains and the Qin−Ba Mountains revealed only sporadic, unidimensional weak-to-moderate trait–constituent correlations, without the formation of stable, systematic associations capable of supporting standardized quality evaluation. This regional divergence in correlations likely stems from differences in geo-authentic background and cultivation practices. As the traditional authentic production region for RAL, the Maoshan region has undergone centuries of natural acclimatization and directed artificial selection, forging a co-evolutionary system linking geo-authentic habitat, distinctive germplasm, stable phenotypic traits, and superior chemotypes. This has consolidated the empirical knowledge that "firm texture, abundant cinnabar-like spots, and strong aroma indicate superior quality". Emerging cultivation regions, however, are affected by diverse ecological conditions, mixed germplasm sources, and insufficient standardization of cultivation management. Compounded by the inherently high genetic diversity of *A. lancea* (e.g., reported genetic similarity of only 0.68 in Dabie Mountain populations [17]), these factors weaken the stable coupling between morphological traits and secondary metabolite accumulation, yielding only fragmented associations.

Collectively, these results suggest that Maoshan-sourced RAL density, R_{cavity}, odor indices, and color parameters (L*) are closely linked to intrinsic bioactive content and can

serve as reliable external indicators for quality assessment. For emerging production areas, priority should be given to standardized germplasm selection and the establishment of standardized cultivation systems before robust, generalizable trait-based quality evaluation frameworks can be developed.

4.2. Density-Based Quality Grading System

The current quality assessment of RAL relies heavily on chromatographic techniques such as GC–MS and HPLC. Although these methods provide accurate quantification, their complex sample preparation, lengthy analysis times, and high costs limit their utility for rapid grading in procurement, market supervision, and routine production settings. In this study, we leveraged the stable trait–constituent relationships established in the traditional authentic production area to develop a three-level density-based grading system (Grade A: $\geq$0.73 g/cm^3; B: 0.58–0.73 g/cm^3; C: <0.58 g/cm^3). This approach transforms the traditional, subjective descriptor of "firm texture" into an objective, quantifiable, and highly reproducible density metric. A single measurement per sample requires only 3 min, demands no specialized equipment or expertise, and is well suited for preliminary screening during medicinal material procurement, market supervision, and pre-processing quality checks by pharmaceutical enterprises.

It should be noted that this grading standard is currently applicable only to 3-year-old cultivated RAL from the Maoshan region, with its reliability predicated on consistency in local ecological conditions and cultivation practices. This grading system cannot be directly extrapolated to RAL samples of different growth ages, under alternative cultivation management modes, or from other geographical origins. The applicability and corresponding threshold values of the system in the above scenarios still require further validation through dedicated empirical studies. In the relatively low-altitude, high-organic-matter soils of Maoshan, RAL develops dense tissues and abundant oil cavities that facilitate the accumulation of bioactive constituents [18]. We tentatively infer that density grading may reflect the plant's adaptive response to its geo-authentic environment and provide a direct, macroscopic reflection of the intrinsic linkage between morphological traits and quality characteristics of authentic medicinal materials. This mechanistic interpretation remains speculative and requires further physiological and ecological evidence for validation. Given the high genetic diversity and variable cultivation practices in emerging production areas, however, the absence of comparable stable correlations currently limits the broader application of this approach.

4.3. Electronic Nose-DFA Geographical Origin Discrimination Model

Although the present study initially focused on correlations between morphological traits and chemical components, with electronic nose analysis serving only as a supplementary tool for odor quantification, we unexpectedly observed pronounced differences in the volatile "odor fingerprints" of RAL across production regions. Sensor response data (Figure 3a) revealed that Maoshan samples exhibited significantly stronger signals on the W1W (terpenes and sulfur compounds), W2W (aromatic and sulfur compounds), and W2S (alcohols, aldehydes, and ketones) sensors compared with those from other producing regions ($p < 0.05$). In contrast, samples from the Dabie Mountains exhibited higher response values on the W5C (short-chain alkanes and aromatic compounds) and W1C (aromatic compounds) sensors. These distinct sensor profiles primarily reflect regional differences in the composition of volatile components, highlighting the potential of electronic nose technology for geographical origin discrimination.

Using these characteristic odor fingerprints, we developed a DFA-based geographical origin discrimination model that achieved a 100% correct classification rate when validated

on 10 independent blind test samples. The approach offers prominent practical advantages: a short detection cycle (<30 min per sample), minimal sample pretreatment, and straightforward operation. It enables rapid on-site origin identification of RAL and provides a reliable new tool for market supervision.

4.4. Novelty and Practical Significance

This study addresses the key limitations of current RAL quality evaluation, namely reliance on subjective empirical judgment and cumbersome instrumental analysis. It makes three distinct contributions in terms of digital trait characterization, on-site quality grading, and rapid origin authentication:

First, this study achieves the first systematic, multi-dimensional digital characterization of RAL morphological traits using integrated multi-sensor techniques. Existing RAL quality studies mostly focus on single-trait indicators such as color [19], lacking a holistic investigation of multiple morphological attributes and their quantitative correlations with bioactive constituents. By integrating colorimetry, image analysis, electronic nose sensing, and density measurement, we comprehensively quantified core traits (density, oil cavity characteristics, color and odor) and systematically elucidated their correlation patterns with four major bioactive components. This work provides rigorous modern analytical chemistry evidence for the traditional principle of Bianzhuang Lunzhi (quality evaluation via morphological traits) and establishes a quantitative link between macroscopic morphological traits and intrinsic chemical quality.

Second, this study develops the first practical single-index quality grading system for RAL, eliminating the dependence of conventional quality assessment on complex chromatographic quantification. Previous quality grading studies on closely related *Atractylodes* medicinal materials [8,20] mostly adopted multi-sensor data fusion combined with chemometric modeling, which involves cumbersome operations and cannot meet the demand for on-site rapid detection. In contrast, based on the strong positive correlation between density and bioactive constituent contents, we established a three-level density grading standard via K-means cluster analysis. This method requires no large-scale analytical instruments, features simple sample pretreatment and good repeatability, and completes a single test within 3 min, making it highly suitable for on-site rapid screening in herbal procurement and market supervision.

Third, this study constructs a rigorous yet practical RAL geographical origin authentication model based on conventional electronic nose sensing. Although electronic nose-based species and origin discrimination of *Atractylodes* materials has been reported, the relevant study employed a flash GC electronic nose coupled with multiple machine learning algorithms [6], which imposes high technical demands on operators and is difficult to extend to routine on-site detection. In this study, we built DFA and PLS-DA discriminant models using odor fingerprints acquired by a conventional electronic nose and adopted a dual validation framework combining leave-one-out cross-validation (LOOCV) and independent blind sample testing. Compared with similar studies relying solely on internal cross-validation, our verification strategy markedly improves model reliability while retaining the advantages of non-destructive and rapid detection, providing a feasible technical tool for on-site origin supervision of commercial RAL.

To further visually demonstrate the advancements and originality of this work relative to existing reports, a systematic comparison with representative studies in this field is summarized in Table S6.

5. Conclusions

This study systematically investigated the morphological traits-bioactive constituent correlation in RAL via multi-sensor characterization and chemometric methods. The main conclusions are as follows:

First, the traditional empirical principle "Bianzhuang Lunzhi" was verified in Maoshan-cultivated RAL, providing modern analytical chemistry evidence for this classical herbal quality evaluation approach. Morphological traits closely reflect the internal quality of Maoshan-sourced RAL: higher density, more abundant oil cavities, stronger aroma, and darker powder color corresponded to higher bioactive component contents.

Second, a density-based three-level quality grading system was established for Maoshan-sourced RAL. This system features rapid detection, simple operation, and good repeatability and is suitable for on-site quality grading in pharmaceutical procurement and market supervision. Notably, the system is currently limited to 3-year-old cultivated RAL from the Maoshan region, and its broader generalizability requires further validation with larger sample sets.

Third, DFA and PLS-DA geographical origin authentication models were developed based on electronic nose odor fingerprints. Both models exhibited reliable discriminative performance, providing practical technical support for origin supervision of commercial RAL.

In summary, this study advances the rapid quality control of RAL from empirical judgment to a data-driven mode and verifies the feasibility and practicality of combining multi-dimensional analytical techniques with chemometrics for traditional herbal medicines quality evaluation. The findings provide feasible tools for the standardized quality control of RAL and also serve as a replicable reference for the quality assessment of other similar herbal medicines.

Supplementary Materials: The following supporting information can be downloaded at https://www.mdpi.com/article/10.3390/chemosensors14070160/s1; Table S1: Sample information of 90 batches of RAL; Table S2: GC-MS method validation parameters of the four target analytes; Table S3: Digitized morphological traits of RAL samples; Table S4: Content determination of key active constituents in RAL samples ($mg \cdot g^{-1}$); Table S5: Comparison of similar studies on quality evaluation and geographical origin authentication of Atractylodes rhizome; Table S6: External validation of the density-based quality grading system using an independent test set (MC31–MC34).

Author Contributions: L.C.: Writing—original draft, Writing—review and editing, Methodology, Conceptualization, Data curation, Supervision, Project administration, Funding acquisition. C.D.: Writing—original draft, Writing—review and editing, Methodology, Visualization, Formal analysis, Data curation. M.W.: Writing—original draft, Validation, Visualization, Data curation, Formal analysis. F.R.: Methodology, Data curation. Z.Z.: Writing—original draft, Formal analysis. H.A.: Writing—review and editing, Conceptualization. All authors have read and agreed to the published version of the manuscript.

Funding: This research and the APC were funded by the Natural Science Foundation of Sichuan Province (grant number 2026NSFSC0630) and the XingLin Scholars Project of Chengdu University of Traditional Chinese Medicine (grant number HBZ2024003).

Institutional Review Board Statement: Not applicable.

Informed Consent Statement: Not applicable.

Data Availability Statement: The original contributions presented in the study are included in the article/Supplementary Material; further inquiries can be directed to the corresponding author.

Acknowledgments: The authors have reviewed and edited the output and take full responsibility for the content of this publication.

Conflicts of Interest: The authors declare no conflicts of interest.

Abbreviations

The following abbreviations are used in this manuscript:

RAL	the dried rhizome of *Atractylodes lancea*
PCA	principal component analysis
DFA	discriminant function analysis
ANOVA	one-way analysis of variance
LOOCV	leave-one-out cross-validation

References

1. Wang, L.; Zhou, L.; Huang, L.; Guo, A. Atractylodis Rhizoma: A review of its traditional uses, phytochemistry, pharmacology, toxicology and quality control. *J. Ethnopharmacol.* **2021**, *266*, 113415. [CrossRef] [PubMed]
2. Kimura, Y.; Sumiyoshi, M. Effects of an *Atractylodes lancea* rhizome extract and a volatile component β-eudesmol on gastrointestinal motility in mice. *J. Ethnopharmacol.* **2012**, *141*, 530–536. [CrossRef] [PubMed]
3. Koonrungsesomboon, N.; Na-Bangchang, K.; Karbwang, J. Therapeutic potential and pharmacological activities of *Atractylodes lancea* (Thunb.) DC. *Asian Pac. J. Trop. Med.* **2014**, *7*, 421–428. [CrossRef] [PubMed]
4. Nakai, Y.; Kido, T.; Hashimoto, K.; Kase, Y.; Sakakibara, I.; Higuchi, M.; Sasaki, H. Effect of the rhizomes of *Atractylodes lancea* and its constituents on the delay of gastric emptying. *J. Ethnopharmacol.* **2003**, *84*, 51–55. [CrossRef] [PubMed]
5. Masuda, Y.; Kadokura, T.; Ishii, M.; Takada, K.; Kitajima, J. Hinesol, a compound isolated from the essential oils of *Atractylodes lancea* rhizome, inhibits cell growth and induces apoptosis in human leukemia HL-60 cells. *J. Nat. Med.* **2015**, *69*, 332–339. [CrossRef] [PubMed]
6. Zhang, C.; Wang, S.; Li, Q.; Zhang, Y.; He, Y.; Yan, B.; Zhou, L.; Guo, L. Metabolomic profiling and chemical marker identification in medicinal plants of *Atractylodes*. *Sci. Tradit. Chin. Med.* **2025**, *3*, 87–95. [CrossRef]
7. Wu, H.; Wang, M.; Zeng, Z.; Dai, C.; Ren, F.; Yin, H.; Chen, L. Data fusion of Fourier transform infrared spectroscopy and high-performance liquid chromatography for the origin identification of different medicinal rhizomes of *Atractylodes*. *Microchem. J.* **2025**, *211*, 113110. [CrossRef]
8. Song, B.; Wang, W.; Liu, R.; Cai, J.; Jiang, Y.; Tang, X.; Wu, H.; Ao, H.; Chen, L. Geographic differentiation of essential oil from rhizome of cultivated *Atractylodes lancea* by using GC-MS and chemical pattern recognition analysis. *Molecules* **2023**, *28*, 2216. [CrossRef] [PubMed]
9. Xie, Z. Theory of 'quality evaluation through morphological identification' in traditional experience-based identification of Chinese medicinal varieties. *Shizhen J. Tradit. Chin. Med. Res.* **1994**, *5*, 263–278. (In Chinese)
10. Lu, L.; Hu, Z.; Hu, X.; Li, D.; Tian, S. Electronic tongue and electronic nose for food quality and safety. *Food Res. Int.* **2022**, *162*, 112214. [CrossRef] [PubMed]
11. Wasilewski, T.; Migoń, D.; Gębicki, J.; Kamysz, W. Critical review of electronic nose and tongue instruments prospects in pharmaceutical analysis. *Anal. Chim. Acta* **2019**, *1077*, 14–29. [CrossRef] [PubMed]
12. Buratti, S.; Malegori, C.; Benedetti, S.; Oliveri, P.; Giovanelli, G. E-nose, e-tongue and e-eye for edible olive oil characterization and shelf life assessment: A powerful data fusion approach. *Talanta* **2018**, *182*, 131–141. [CrossRef] [PubMed]
13. Gupta, T.; Yellishetty, M.; Singh, T.N. Measurement of bulk volume and density of irregular solid samples by sand displacement method. *Rock Mech. Rock Eng.* **2017**, *50*, 639–645. [CrossRef]
14. Jentzsch, M.; Albiez, V.; Kardamakis, T.C.; Speck, T. Analysis of the peel structure of different *Citrus* spp. via light microscopy, SEM and CT with manual and automatic segmentation. *Soft Matter* **2024**, *20*, 2804–2811. [CrossRef] [PubMed]
15. Wang, M.; Fei, C.; Zhou, Y.; Dai, Y.; Ren, L.; Zhang, X.; Yin, F. Effect of chemical components on color variation during processing of Crataegi Fructus. *Food Sci. Biotechnol.* **2024**, *33*, 3245–3255. [CrossRef] [PubMed]
16. Zhang, L.; Ouyang, Z.; Zhao, M.; Wang, P.; Wei, Y.; Fang, J. Simultaneous determination of atractylone, hinesol, β-eudesmol, and atractylodin in *Atractylodes lancea* and its cluster analysis. *Chin. J. Nat. Med.* **2010**, *35*, 725–728. (In Chinese) [CrossRef]
17. Guo, L.; Huang, L.; Jiang, X.; Zhan, Y. RAPD analysis of genetic structure of *Atractylodes lancea*. *Chin. Pharm. J.* **2006**, *3*, 178–181. (In Chinese) [CrossRef]
18. Wang, H.; Peng, Z.; Zhang, C.; Kang, C.; Zhang, Y.; Guo, X.; Wang, Y.; Yang, G.; Xiang, Z.; Zhou, L.; et al. The combined influence of microbiome and soil environment contributes to the chemotype differentiation in *Atractylodes lancea*. *iMetaOmics* **2025**, *4*, e70058. [CrossRef] [PubMed]

19. Feng, J.X.; Wu, Y.Z.; Li, S.Y.; Chang, A.; Yu, Q.X.; Zhang, H. Correlation between active component content and color of *Atractylodes lancea* and *A. chinensis* based on color difference principle. *Chin. J. Chin. Mater. Med.* **2023**, *48*, 2086–2091. (In Chinese) [CrossRef] [PubMed]
20. Zhang, C.; Wang, H.; Lyu, C.; Wang, Y.; Sun, J.; Zhang, Y.; Xiang, Z.; Guo, X.; Wang, Y.; Qin, M.; et al. Authenticating the geographic origins of *Atractylodes lancea* rhizome chemotypes in China through metabolite marker identification. *Front. Plant Sci.* **2023**, *14*, 1237800. [CrossRef] [PubMed]